Supporting information

# Improving the reducibility of $CeO_2/TiO_2$ by high-temperature redox treatment: key role of atomically thin $CeO_2$ surface layers.

Ramón Manzorro, José M. Montes-Monroy, D. Goma, José J. Calvino, José A. Pérez-Omil*, Susana Trasobares.

Departamento de Ciencia de los Materiales e Ingeniería Metalúrgica y Química Inorgánica, Facultad de Ciencias, Universidad de Cádiz, Campus Río San Pedro, Puerto Real, 11510 Cádiz, Spain

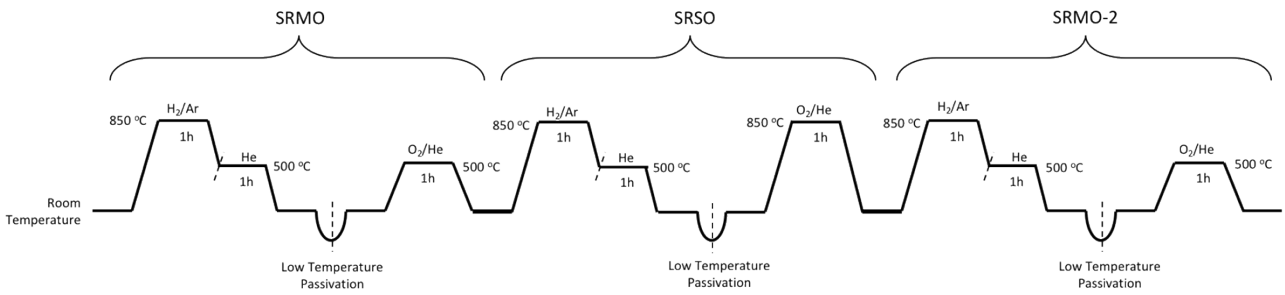


**Figure S1**. Scheme describing the procedure (gas environment and temperature) applied to the $CeO_2/TiO_2$-fresh sample. The first Severe-Reduction Mild-Oxidation (SRMO) gave rise to the $CeO_2/TiO_2$-SRMO-1C sample. Subsequent Severe-Reduction Severe Oxidation (SRSO) led to the formation of the $CeO_2/TiO_2$-SRSO-2C sample, and finally the posterior SRMO-2 treatment brought the $CeO_2/TiO_2$-SRMO-3C sample. All the severe treatments have been accomplished at 850 ºC and mild treatments at 500 ºC, in $H_2$/Ar the case of reductions and $O_2$/He for oxidations.

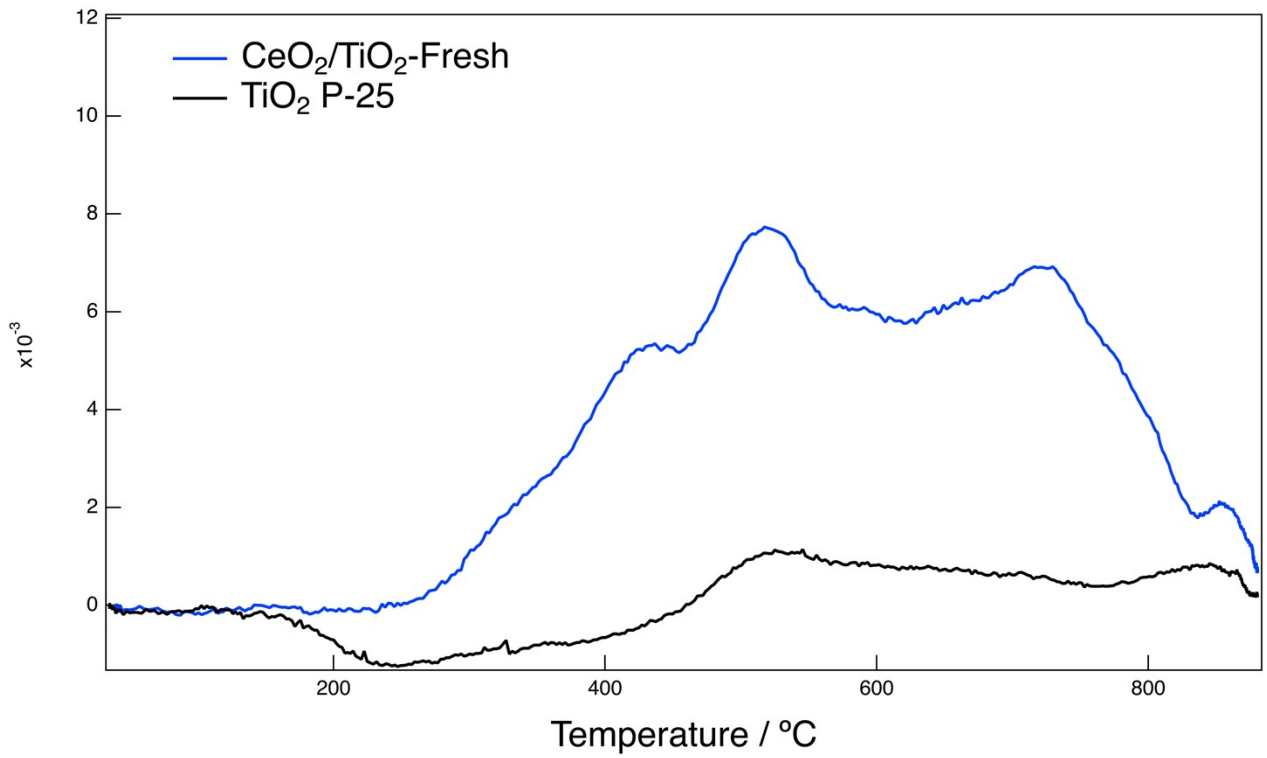


**Figure S2**. TPR-TCD profiles corresponding to the $TiO_2$-P25 bare sample (black line), superimposed corresponding to the TPR-TCD of the $CeO_2/TiO_2$-fresh sample (blue line). Compared to the as-synthesized sample, the $TiO_2$ support shows a minor reduction degree, starting at ~500 $^{o}$C with an almost constant low profile onwards.

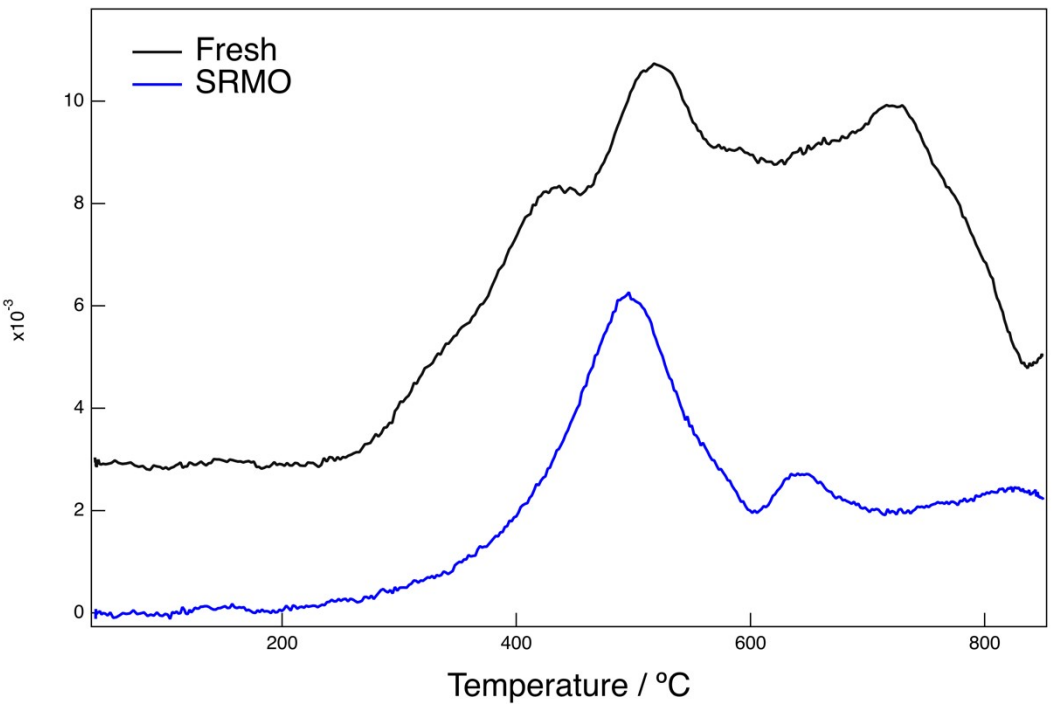


**Figure S3**. Quantitative TPR-TCD corresponding to the $CeO_2/TiO_2$-fresh (black line) and $CeO_2/TiO_2$-SRMO-1C (blue line). $H_2$ consumptions after considering the slight $TiO_2$ reduction, give rise to 0.29 and 0.16 mmol $H_2$/g respectively.

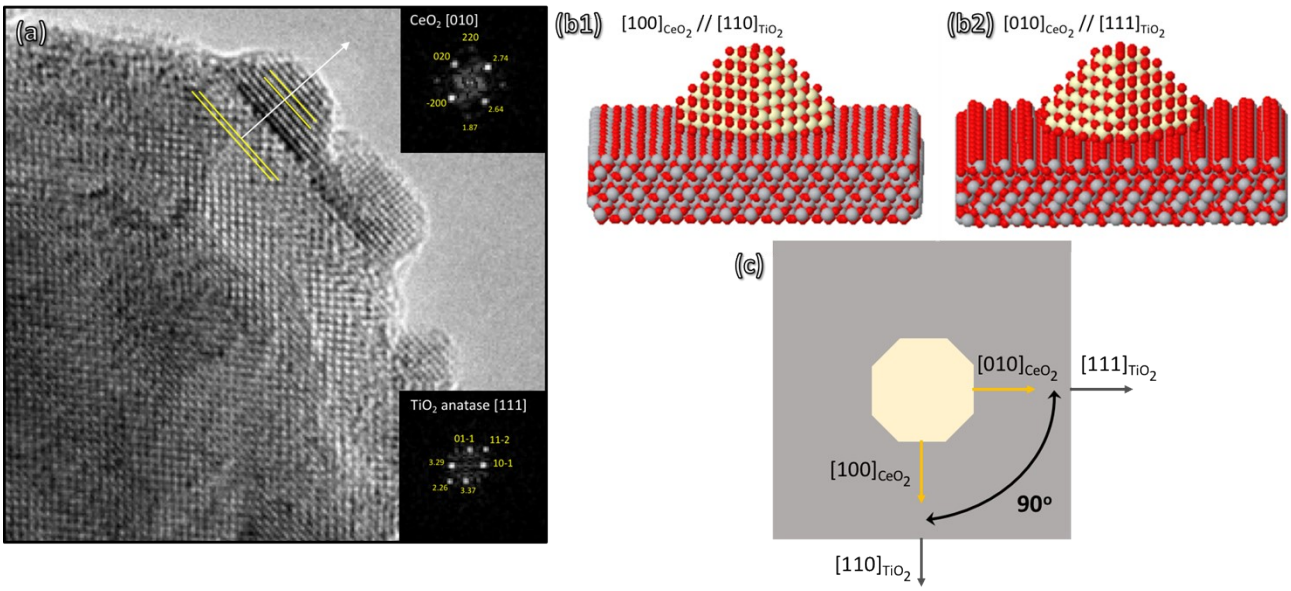


**Figure S4**. $CeO_2/TiO_2$ structural relationship. (a) Experimental HRTEM image illustrating a couple of small $CeO_2$ nanoparticles deposited over a $TiO_2$ anatase particle where the white arrow shows the epitaxial growth of the planes indicated with yellow lines, (200) for $CeO_2$ along [010] and $(11\underline{2})$ for $TiO_2$ along [111]. (b) $CeO_2/TiO_2$ atomic models describing the structural relationship: (b1) represent the epitaxy reported in the bibliography taking place from the along the [100] and [110] zone axis in $CeO_2$ and $TiO_2$ respectively, meanwhile (b2) depicts the same structural relationship from directions [010] in $CeO_2$ and [111] in $TiO_2$, characterized in our present work. (c) Scheme revealing the 90º relationship between the two situations described in atomic models.

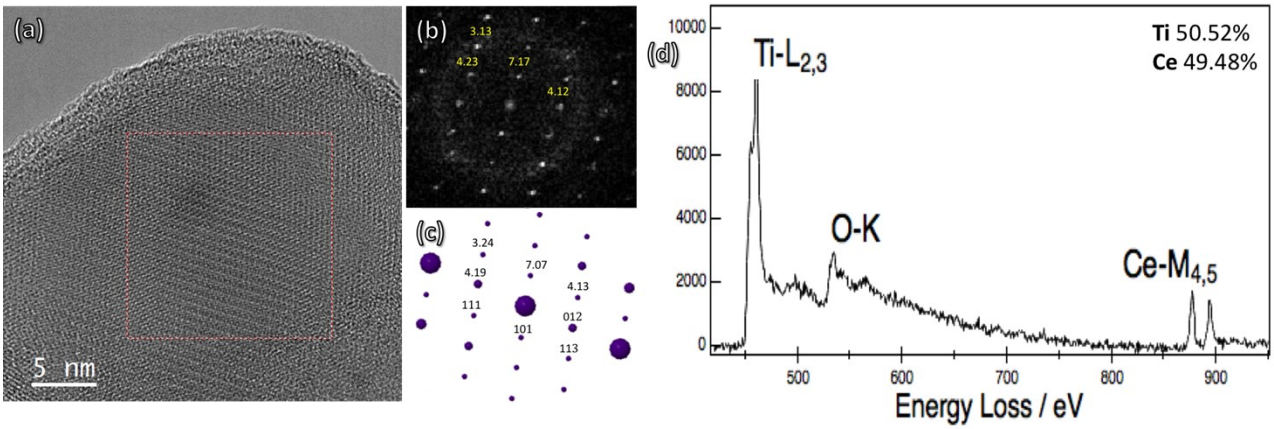


**Figure S5**. $Ce_2Ti_2O_7$ structure. (a) HREM image corresponding to a $Ce_2Ti_2O_7$ perovskite oriented in the [121] direction. (b) Digital diffraction pattern extracted from the region marked with a doted box on the $Ce_2Ti_2O_7$ crystal. (c) Theoretical diffraction pattern for this structure on the [121] direction, showing same reflections that the ones observed on the experimental one, confirming the structure and the zone axis. (d) EELS spectrum acquired over the crystal under study. Quantification through Ti-$L_{2,3}$ and Ce-$M_{4,5}$ edges points out a 1:1 proportion on the Ce:Ti ratio, as expected for the structure $Ce_2Ti_2O_7$.

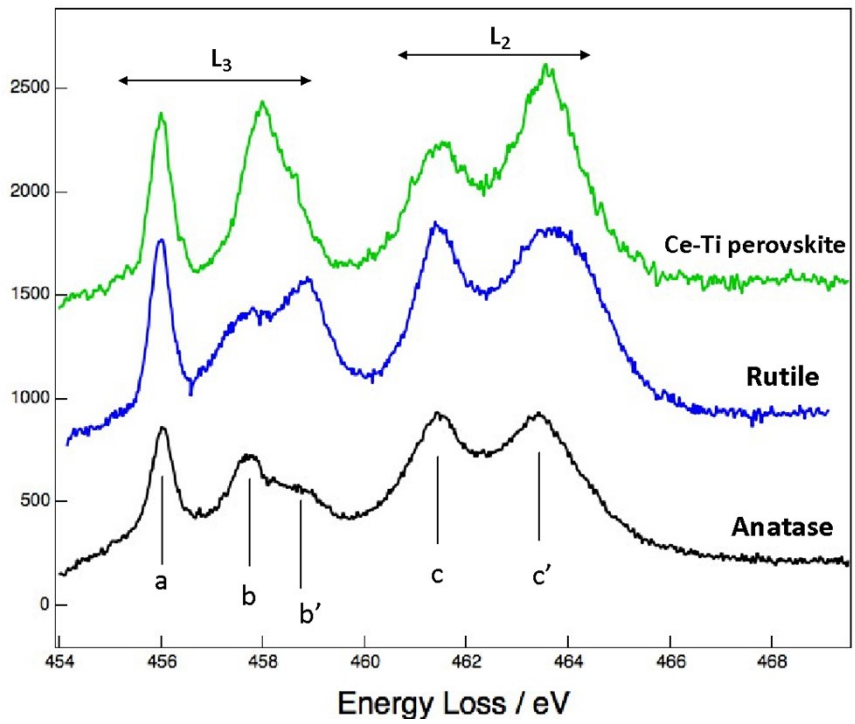


**Figure S6**. Analysis of the ELNES structure. The graph gathers from bottom to top the Ti-$L_{2,3}$ edge of anatase, rutile and Ce-Ti bulk-type mixed oxide phases. As compared to the well-reported anatase and rutile structure, the mixed oxide spectrum does not present a splitting in the $e_g$ series of the $L_3$ edge, but a single and intense peak instead.

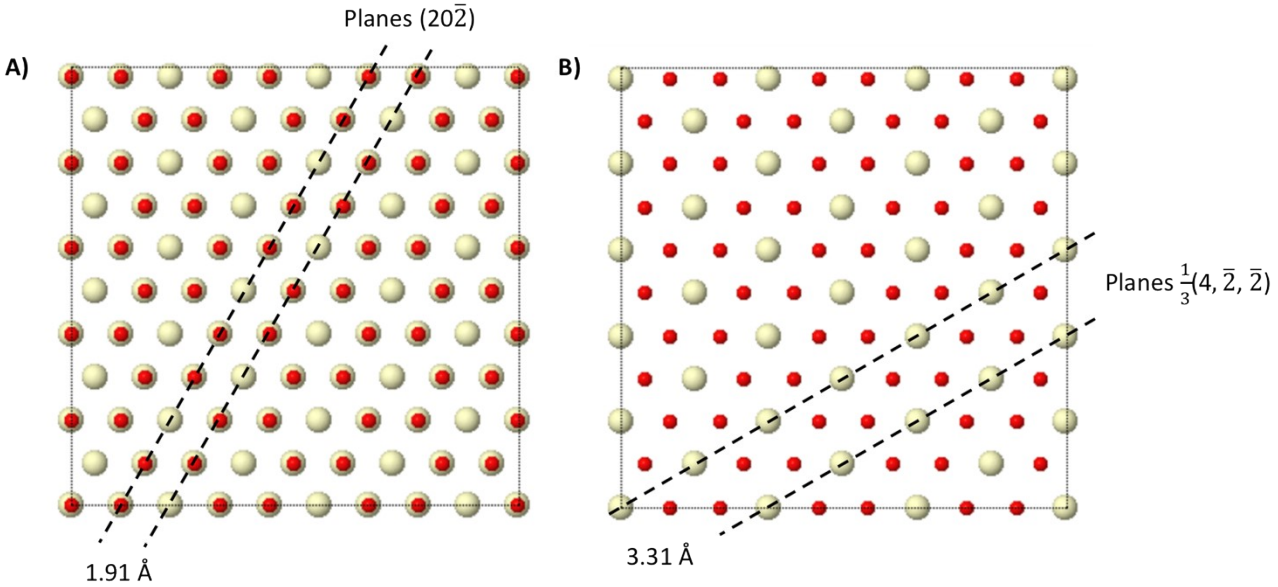


**Figure S7**. Atomic models corresponding to (111)-$CeO_2$ planes. (a) Top view of 3 (111)-$CeO_2$ facets stacks in a conventional ABC arrangement for fluorite. As indicated, the planes (20$\bar{2}$) are separated by 1.91 Å. (b) In contrast, the planes taking place, and therefore, the spacings, in a single (111)-$CeO_2$ facet are different compared to the ABC stacked structure. For a single (111) layer, the planes observed are 1/3(4$\bar{2}\bar{2}$), with larger spacings, 3.31 Å, equivalent to the (100) reflection for the trigonal A-$Ce_2O_3$ structure. These atomic models consider the 5.41 Å characteristic lattice parameter for $CeO_2$ bulk.

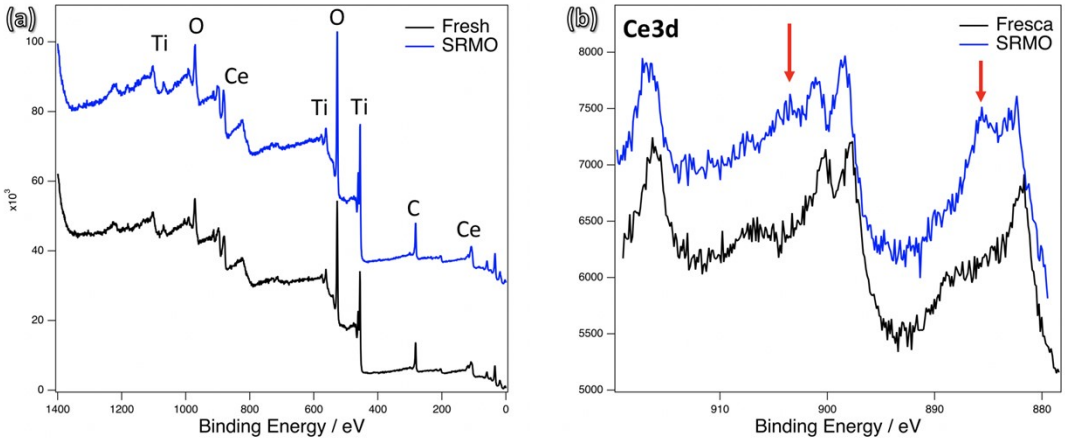


(c) XPS results for $CeO_2/TiO_2$-fresh and $CeO_2/TiO_2$-SRMO-1C samples

| | Ce/Ti | $Ce^{3+}/Ce^{4+}$ (short) | $Ce^{3+}/Ce^{4+}$ |
|---|---|---|---|
| Fresh | 0.202 | 0.20 | 0.61 |
| SRMO | 0.195 | 0.41 | 1.53 |

(d) Angle-resolved XPS performed on the $CeO_2/TiO_2$-SRMO-1C samples

| Angle | 75 | 60 | 45 | 30 | 15 |
|---|---|---|---|---|---|
| Ce/Ti | 0.18 | 0.18 | 0.18 | 0.19 | 0.20 |

**Figure S8**. Summary of the XPS analysis carried out on the $CeO_2/TiO_2$-fresh and $CeO_2/TiO_2$-SRMO-1C. (a) Survey (0-1400 eV) XPS spectra of the fresh (black line) and SRMO (blue line) samples, where the main peaks corresponding to Ce, Ti, O and C have been labelled. (b) High-resolution spectra of Ce-3d. Red arrows indicate the main contribution of $Ce^{3+}$, much more evident for the SRMO sample. (c) Ce/Ti and $Ce^{3+}/Ce^{4+}$ molar ratios quantified from XPS spectra. (d) Angle-resolved Ce/Ti molar ratio obtained for different incident angles.

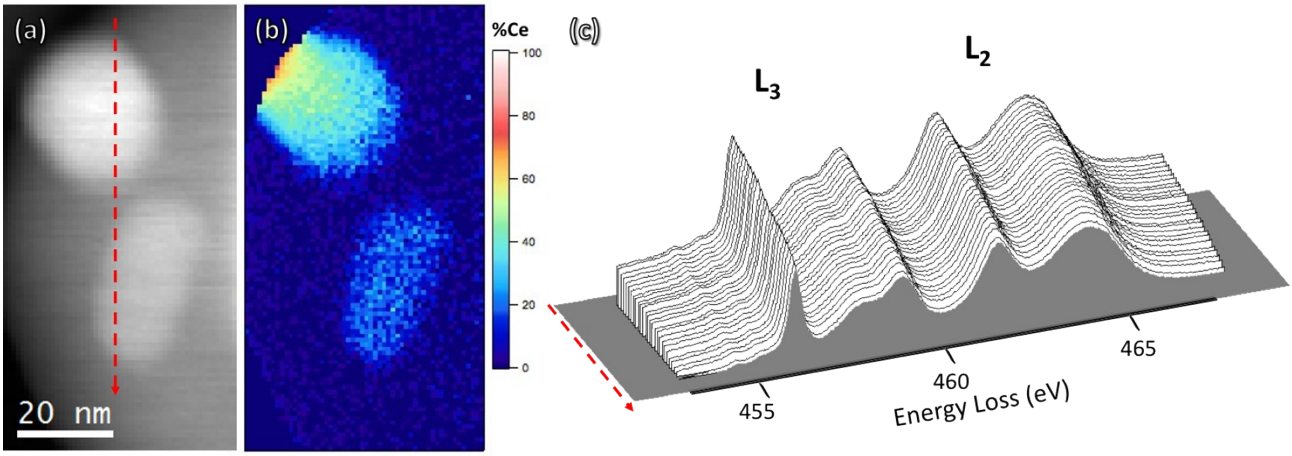


**Figure S9**. Analysis of the ELNES structure for the $CeO_2/TiO_2$-SRSO-2C sample. (a) Representative ADF image illustrating two bright regions with a high content of Ce, as observed in the elemental map (b) built with the Ce-$M_{4,5}$ edge. (c) Ti-$L_{2,3}$ fine structure registered across the red arrow on the ADF image. The ELNES analysis points out that, even though the content of cerium is high, the Ti-$L_{2,3}$ structure remains on its rutile phase. This fact suggests the cerium and titanium are not forming a mixed oxide but instead ceria particles supported on rutile-like titania crystals.

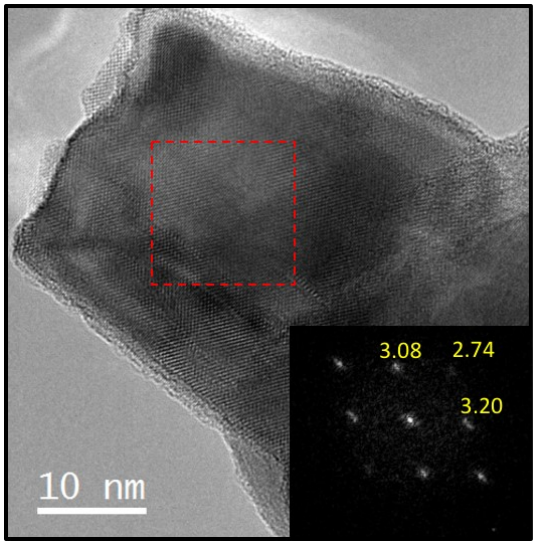


**Figure S10**. Fluorite-type $CeO_2$ crystal corresponding to the $CeO_2/TiO_2$-SRSO-2C sample. The digital diffraction pattern acquired on the red box presented as an inset on the image, indicates that the particle is oriented along the [011] zone axis.